Electronic and Optical Excitations of Aminopyrimidine Molecules from Many-Body Perturbation Theory

A. Riefer, M. Rohrmüller, M. Landmann, S. Sanna, E. Rauls, U. Gerstmann, and W.G. Schmidt

Abstract Calculations based on (occupation constrained) density functional theory using local as well as hybrid functionals to describe the electron-electron exchange and correlation are combined with many-body perturbation theory in order to determine the electronic and optical excitation properties of 5-(pentafluorophenyl)pyrimidin-2-amine, 5-(4-methoxy-2,3,5,6-tetrafluorophenyl)-pyrimidin-2-amine, and 5-(4-(dimethylamino)-2,3,5,6-tetrafluorophenyl)pyrimidin-2-amine. Large quasiparticle shifts and exciton binding energies of about 4 eV are found. They cancel each other partially and thus allow for a meaningful description of the molecular optical response within the independent-particle approximation. We find a surprisingly strong influence of local-field effects as well as resonant-nonresonant coupling terms in the electron-hole Hamiltonian on the optical properties.

1 Introduction

Organic semiconductors are important materials for various applications due to their low cost fabrication processes and the possibility to fine-tune desired functions by chemical modification of their building blocks. While the last years have seen a tremendous progress in the understanding of the excitation properties of inorganic semiconductors, fueled in part by the availability of advanced computational schemes for electronic structure and optical response calculations such as the GW approximation (GWA) for obtaining accurate electronic quasiparticle energies and

A. Riefer · M. Rohrmüller · M. Landmann · S. Sanna · E. Rauls · U. Gerstmann ·
W.G. Schmidt (✉)
Lehrstuhl für Theoretische Physik, Universität Paderborn, 33095 Paderborn, Germany
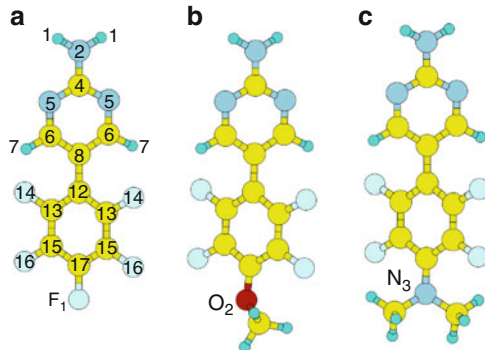e-mail: W.G.Schmidt@upb.de

Fig. 1 Schematic model of 5-(pentafluorophenyl)pyrimidin-2-amine (FAP), 5-(4-methoxy-2,3,5,6-tetrafluorophenyl)pyrimidin-2-amine (OFAP), and 5-(4-(dimethylamino)-2,3,5,6-tetra-fluorophenyl)pyrimidin-2-amine (NFAP) (from left to right). *Dark (red), light (yellow), gray, lightgray* and *small balls* indicate O, C, N, F and H atoms, respectively

the Bethe-Salpeter approach (BSE) to calculate electron-hole interaction effects [1–6], far less is known about the electronic and optical properties of organic crystals.

Recently, a novel class of organic electronic material has been synthesized by the self-assembly and silver(I) complex formation of 2-aminopyrimidines [7]. The compounds were structurally as well as optically characterized [8] and it was found that the solid state absorption differs remarkably from the parent compound 2-aminopyrimidine. The optical properties could be tuned by changing the silver counterion or by the reversible solvent extrusion and interchange. Furthermore, the electrical conductivity of the material was proven for a thin crystalline film.

In order to gain a better understanding of the excitation properties of this class of systems, we first study molecular excitations in the respective parent molecules. In detail, we present *first-principles* calculations on the electronic and optical properties of 5-(pentafluorophenyl)pyrimidin-2-amine (FAP), 5-(4-methoxy-2,3,5,6-tetrafluorophenyl)pyrimidin-2-amine (OFAP), and 5-(4-(dimethylamino)-2,3,5,6-tetrafluorophenyl)pyrimidin-2-amine (NFAP) in order to clarify the impact of many-body effects and chemical trends. The three aminopyrimidine molecules (APM) are shown in Fig. 1. They consist of 22 (FAP), 26 (OFAP) and 30 (NFAP) atoms forming a 2-aminopyrimidine ring (atoms 1–8 in Fig. 1) and a (per)fluorinated phenylring ring (12–17) where the position no. 22 is either a fluorine atom F_1 (FAP), a methoxy group (OFAP) or an amino group (NFAP).

2 Methodology

Ground-state and GWA calculations are performed using the Vienna Ab-initio Simulation Package (VASP) implementation [9] of the gradient-corrected [10] density functional theory (DFT-GGA). In addition, the hybrid functional due to

Heyd, Scuseria, and Ernzerhof (HSE06) [11] was used. The electron-ion interaction is described by the projector augmented-wave (PAW) method [12, 13]. We expand the valence wave functions into plane waves up to an energy cutoff of 400 eV. DFT calculations for single molecules were performed using a $14 \times 15 \times 20 \text{ Å}^3$ super cell and Γ point sampling for the Brillouin zone (BZ) integration. Test calculations show that the eigenenergies are converged within a few hundredths an eV. For electronic self-energy calculations applying perturbation theory ($G_0 W_0$) and Bethe-Salpeter type calculations (see, e.g., Ref. [5]) as well as for calculations of charged molecules the cell size was varied as described below.

DFT calculations are known to often considerable underestimate electronic excitation energies [4]. Reliable quasiparticle gaps, exciton pair energies and Stokes shifts, however, can be obtained from occupation constraint DFT (or ΔSCF) methods, cf. Refs. [14–16]. Thereby the quasiparticle (QP) gap is obtained directly as difference between the ionization energy and electron affinity

$$E_g^{QP} = E(N+1, \mathbf{R}) + E(N-1, \mathbf{R}) - 2E(N, \mathbf{R}), \tag{1}$$

where $E(N, \mathbf{R})$, $E(N+1, \mathbf{R})$, and $E(N-1, \mathbf{R})$ represent the energy of a N, $N+1$, and $N-1$ electron system, respectively, with the equilibrium geometry $\mathbf{R}$ of the N electron system. The energy of the lowest excitonic excitation corresponding to the situation that one electron occupies the lowest unoccupied molecular orbital (LUMO) leaving a hole behind in the highest occupied molecular orbital (HOMO) is given by

$$E_{ex} = E(e-h, \mathbf{R}) - E(N, \mathbf{R}), \tag{2}$$

where $E(e-h, \mathbf{R})$ is the total energy of the system in presence of the electron-hole-pair with fixed geometry $\mathbf{R}$. Alternatively, as can be derived from Janak's Theorem (see Ref. [14]), the energy of the lowest optical excitation can be obtained from the difference of the eigenenergies of the half-occupied HOMO $\varepsilon_{H,0.5}$ and LUMO $\varepsilon_{L,0.5}$, respectively

$$E_{ex} \simeq E_{ex}^J = \varepsilon_{L,0.5} - \varepsilon_{H,0.5}. \tag{3}$$

Relaxing the atomic coordinates to the geometry $\mathbf{R}^*$ for fixed occupation numbers yields the lowest emission energy

$$E_{em} = E(e-h, \mathbf{R}^*) - E(N, \mathbf{R}^*), \tag{4}$$

which can be used to calculate the Stokes shift

$$\Delta_S = E_{ex} - E_{em}. \tag{5}$$

From calculations of the ground-state energy for different cell sizes one can conclude an error for the ΔSCF values of 0.1 eV. The QP gaps E_g^{QP} are compared to the gap $E_g^{G_0 W_0}$ that has been obtained from the $G_0 W_0$ approximation of the electronic self energy and is obtained by postprocessing the PW91 wave functions and eigenvalues. The implementation details are given in Ref. [17].

For systems where the electronic states have either the occupancy 0 for conduction states, $n = c$, or 1 for valence states, $n = v$ one obtains the dielectric tensor in independent-particle approximation [18–20] (IPA)

$$\varepsilon_{ij}(\omega) = \delta_{ij} + \frac{4\pi e^2}{\Omega} \lim_{\mathbf{q}\to 0} \frac{1}{q^2} \sum_{\mathbf{k}cv} 2$$

$$\times \frac{1}{\varepsilon_c(\mathbf{k}) - \varepsilon_v(\mathbf{k}) - (\hbar\omega + i\eta)} \langle u_{c\mathbf{k}+\mathbf{q}_i} | u_{v\mathbf{k}} \rangle \langle u_{c\mathbf{k}+\mathbf{q}_j} | u_{v\mathbf{k}} \rangle^*, \qquad (6)$$

where the sum $\sum_{\mathbf{k}}$ is to be taken over the first BZ, $\mathbf{q}_i$ is the reciprocal vector in the cartesian direction i, $u_{n\mathbf{k}}$ are the periodic parts of the Bloch wave functions, $\varepsilon_n(\mathbf{k})$ the respective eigenenergies, Ω is the crystal volume, and η is the broadening. In order to allow for comparison with the experimental data we average over the three cartesian directions

$$\varepsilon(\hbar\omega) = \frac{1}{3} \sum_{i=x,y,z} \varepsilon_{ii}(\hbar\omega). \qquad (7)$$

The dielectric function within the IPA or by solving the BSE is based on the electronic structure as obtained from either the PW91/HSE06 calculations (partially with scissors shifted eigenvalues) or from the GWA.

Solving the Bethe-Salpeter equation includes the electron-hole attraction and local-field effects in the dielectric function. For practical calculations, the BSE is transformed into a two-particle Schrödinger equation. Neglecting dynamical screening and umklapp processes, the resonant part of the exciton Hamiltonian (Tamm-Dancoff-Approximation, TDA, cf. Ref. [21]) for direct transitions and spin-singlets can be calculated in reciprocal space according to

$$\hat{H}^{res}_{vc\mathbf{k},v'c'\mathbf{k}'} = (\varepsilon_c^{QP}(\mathbf{k}) - \varepsilon_v^{QP}(\mathbf{k}))\delta_{vv'}\delta_{cc'}\delta_{\mathbf{k}\mathbf{k}'}$$

$$+ \frac{4\pi}{\Omega} \sum_{\mathbf{G},\mathbf{G}'} \Big\{ 2\frac{\delta_{\mathbf{G}\mathbf{G}'}(1 - \delta_{\mathbf{G}0})}{|\mathbf{G}|^2} B^{\mathbf{k}\mathbf{k}}_{cv}(\mathbf{G}) B^{\mathbf{k}'\mathbf{k}'*}_{c'v'}(\mathbf{G})$$

$$- \frac{\varepsilon^{-1}(\mathbf{k} - \mathbf{k}' + \mathbf{G}, \mathbf{k} - \mathbf{k}' + \mathbf{G}', 0)}{|\mathbf{k} - \mathbf{k}' + \mathbf{G}|^2} B^{\mathbf{k}\mathbf{k}'}_{cc'}(\mathbf{G}) B^{\mathbf{k}\mathbf{k}'*}_{vv'}(\mathbf{G}') \Big\}, \qquad (8)$$

where the Bloch integral

$$B^{\mathbf{k}\mathbf{k}'}_{nn'}(\mathbf{G}) = \frac{1}{\Omega} \int d\mathbf{r} u^*_{n\mathbf{k}}(\mathbf{r}) e^{i\mathbf{G}\mathbf{r}} u_{n'\mathbf{k}'}(\mathbf{r}) \qquad (9)$$

over the periodic parts u of the Bloch wave functions has been introduced. In the actual calculations we replace the inverse dielectric matrix ε^{-1} by a diagonal model dielectric function suggested by Bechstedt et al. [22]. It depends on the static dielectric constant ε_∞ and reduces the computational effort substantially. In case of inorganic semiconductors [23, 24], molecular crystals [16, 25] and even surfaces

[26], the application of this model dielectric function leads to rather accurate results. This is related to the fact that the model dielectric function depends on the local charge density and therefore carries some information about the local screening. For molecule calculations, the correct choice of ε_∞ is difficult. The authors of Ref. [27] defined an effective volume Ω_{eff} where the screening takes place in order to address this problem in their optical response calculation of poly-para-phenylenevinylene. In our work we use for molecular calculations $\varepsilon_\infty = 1$, which marks the lower limit for the screening interaction. If one assumes $\Omega_{eff} = 18^3$ Å^3, the IPA calculations for FAP result in $\varepsilon_\infty = 1.05$, which leads to a blueshift of the excitonic eigenvalues by about 0.3 eV. Calculations for further values of ε_∞ indicate a nearly linear dependence of the exciton binding energies on the screening, as may be expected. The dimension of the exciton Hamiltonian (Eq. 8) is determined by the size of the energy window for conduction and valence states. The spectra are calculated including either all states satisfying $\varepsilon_c(\mathbf{k}) - \varepsilon_v(\mathbf{k}) < 6$ eV (DFT) or the lowest 96 states (GWA). For the actual calculation of the spectra we use the time-evolution algorithm proposed by one of the present authors [26]. In addition to BSE-TDA, also calculations with the full exciton Hamiltonian were performed (BSE). For the comparison with measured optical spectra we use real and imaginary parts of the dielectric function, $\varepsilon'(\hbar\omega)$ and $\varepsilon''(\hbar\omega)$, respectively to obtain the attenuation coefficient α using the approximation

$$\alpha(\hbar\omega) \propto \hbar\omega \sqrt{\left[\sqrt{\varepsilon'(\hbar\omega)^2 + \varepsilon''(\hbar\omega)^2} - \varepsilon'(\hbar\omega) \right]}. \qquad (10)$$

The calculated data are compared with optical absorption measurements on powder samples.

The HLRS CRAY XE6 is the main computational resource used for the calculations in this work. As can be seen in Fig. 2, the scaling is nearly linear up to 200 cores, allowing for highly efficient calculations.

3 Results

The structural relaxation of FAP, OFAP and NFAP in gas phase shows that the geometry of the aminopyrimidine and pentafluorophenyl rings does barely change upon attachment of either a fluorine atom (FAP), a methoxy group (OFAP) or an amino group (NFAP). The comparison of our calculated data with x-ray data of two polymorphic crystals of the hydrogen analogue 5-phenyl-pyrimidin-2-ylamine (HAP) and a HAP-hexafluorobenzene co-crystal[7] as well as the recently crystallized NFAP ligand itself shows only small differences in bond length and angles. Only for the hydrogen bonds we observe deviations of up to 0.10–0.16 Å between measured and calculated data. The geometries calculated here also closely agree with Møller Plesset perturbation theory (MP2) results for APM [28]: The bond lengths deviate by less than 0.02 Å and the largest deviation of bond angles amounts to 3°.
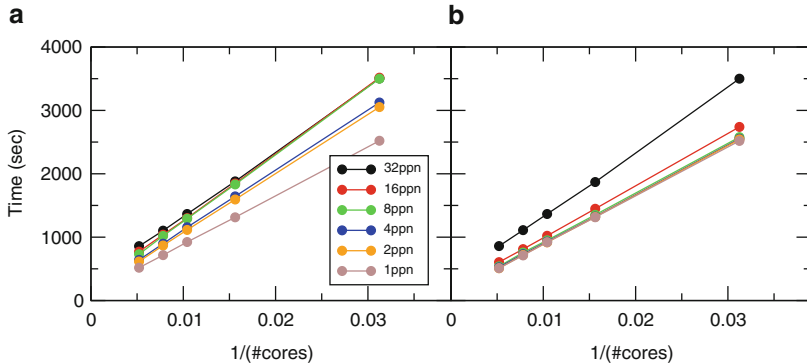
a

b

Fig. 2 Wall clock time for the DFT-GGA calculation of 5-(pentafluorophenyl)pyrimidin-2-amine (FAP) in a $20 \times 20 \times 20$ Å^3 cell including 1,152 electronic states on the HLRS CRAY XE6. In (**a**) the behavior of the wall clock time with respect to the number of cores and tasks per node (*ppn*) is shown. As can be seen, the scaling is nearly linear up to 200 cores. The time required is reduced with increased distribution of the tasks on several nodes. Additionally, (**b**) shows that the wall clock time can be further reduced if the cores employed for the calculations are equally spaced (spacing 32/#ppn) on the nodes

Table 1 Molecular excitation energies (in eV, see text)

	FAP	OFAP	NFAP
E_g^{PW91}	3.46	3.35	3.00
E_g^{HSE06}	4.53	4.55	4.21
$E_g^{G_0W_0}$	$\lesssim 7.7$	$\lesssim 7.4$	$\lesssim 7.1$
E_g^{QP}	7.36	7.06	6.47
E_{ex}	3.51	3.46	3.21
E_{ex}^J	3.50	3.46	3.22
E_{em}	2.08	1.97	1.98
Δ_S	1.43	1.49	1.23

Starting from the relaxed structures we calculated the quantities defined in Eqs. (1)–(5). The results for FAP, OFAP, and NFAP are compiled in Table 1. We find that the difference of the HOMO and LUMO eigenenergies, $E_g^{PW91} = \varepsilon_L - \varepsilon_H$, is largest for FAP and decreases by going from OFAP to NFAP (see also Fig. 4 for the electronic levels), i.e., with increasing electron-donating properties. In HSE06 the ordering between FAP and OFAP is reverse compared to the GGA calculation. However, the gaps are very close. The trend observed with GGA holds also for the G_0W_0 gaps $E_g^{G_0W_0}$ and the ΔSCF gaps E_g^{QP}. The calculation of a QP ΔSCF gap requires the determination of the total energies $E(N + 1, \mathbf{R})$ and $E(N - 1, \mathbf{R})$ of charged molecules. Due to the interactions with the periodic images the dependence of the latter and thus the gap E_g^{QP} on the cell size is not negligible. In order to correct the calculated excitation energies, the gaps were determined for a cubic cell with varying size $L = 18, \ldots, 30$ Å.

As shown in Fig. 3, the gap values depend linearly on $1/L$. Extrapolation to $L \to \infty$ leads to the gaps cited in Table 1.
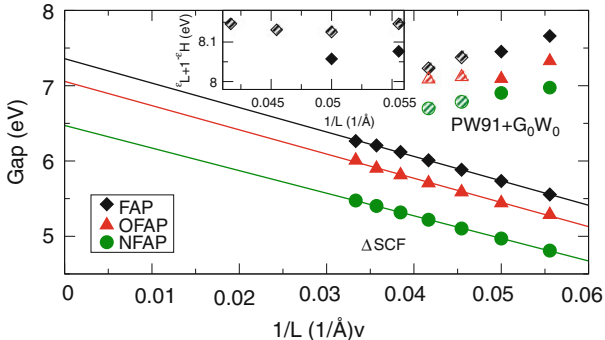
Fig. 3 Dependence of the calculated quasiparticle-gaps E_g^{QP} and G_0W_0 gaps $E_g^{G_0W_0}$ on the cell size L. The filled/striped symbols for G_0W_0 values denote calculations with a cutoff for the response function of $60/40$ eV (see text). The inset shows the respective values for the energy difference between the LUMO+1 and HOMO

A dependence on the unit cell size is also noted for the calculated G_0W_0 gaps, see Fig. 3. To some extent, this is to be expected due to the periodic repetition of the molecules. The restriction of the calculations with respect to further parameters due to numerical limitations, however, is even more important in the present case. The self-energy calculations for cubic cells with the size $L = 18$–20 Å (22–24 Å) were performed with a maximum cutoff for the response function of 60 eV (40 eV), 90 frequency points, and a cutoff of 15–16 eV for the sum over empty states (including up to 1,056 bands).

The dependence of the G_0W_0 on the numerics is obvious from the inset in Fig. 3, where the energy difference between the FAP HOMO and LUMO+1 states is shown, but also from Fig. 4, where the energetic ordering of the electronic states is visualized. Obviously, the order changes upon inclusion of electronic self-energies calculated with the G_0W_0 approximation, but is itself not yet converged, at least for the unoccupied states. Nevertheless, as will shown below, the reordering due to state-dependent self-energy corrections calculated in G_0W_0 improves the agreement between the measured and calculated optical absorption. The present data suggest that the band gaps calculated within the GWA decrease with increasing cell size for the molecules studied here. The numbers given in Table 1 should thus be considered as approximate upper limits. We find that the values are by about 0.5 eV larger than the respective energy gaps determined from the ΔSCF calculations. The fundamental gaps calculated with the HSE06 scheme, on the other hand, are between the PW91 and the quasiparticle gaps.

Interestingly, the quasiparticle shifts are nearly cancelled by electron-hole attraction effects: The lowest electron-hole excitation energies E_{ex} are remarkably close to the difference of the HOMO and LUMO single particle eigenenergies obtained from DFT. This near cancellation of many body effects due to the electron-electron and the electron-hole interaction suggests that optical excitation spectra calculated
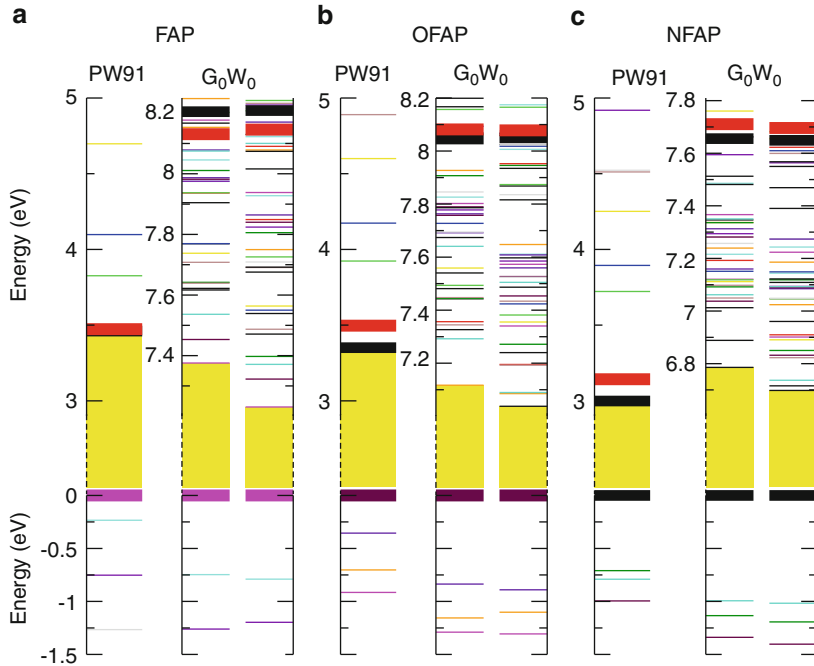
Fig. 4 Energies of molecular orbitals as obtained from DFT (PW91) and G_0W_0 calculations for cubic cells with $L = 22$ Å (*left*) and $L = 24$ Å (*right*). The influence of the self-energy corrections and cell size on the energy order of the states is indicated by different colors. *Thick bars* refer to the orbitals that correspond to HOMO, LUMO, and LUMO+1 in the PW91 calculations. The fundamental gap is indicated. Note the different energy-region for the empty states

in the independent-particle approximation may be a reasonable description at least for the low-energy excitations.

The calculation of the electron-hole excitation energies is computationally robust: The approaches according to Eqs. (2) and (3) result in energies that agree within 0.01 eV. The lowest-energy excitations calculated for structural relaxation differ appreciable from the respective vertical excitation energies. We calculate Stokes shifts between 1.2 and 1.5 eV for the three molecules. Thereby, the energetic ordering changes between absorption and emission. While NFAP is predicted to have the lowest vertical excitation energy, its deexcitation occurs at slightly larger energies than OFAP.

Our calculated values are in reasonable agreement with the experimental data available: For FAP dissolved in ethanol Stoll et al.[8] measured a Stokes shift of 1.28 eV. Given that the optical response of the molecules will be influenced by the solvent, these data confirm the validity of the present calculations.

From the eigenfunctions and eigenvectors obtained in DFT one can directly calculate the dielectric function in independent-particle approximation. Figure 6 shows the resulting spectra for FAP, OFAP, and NFAP. Obviously, in all three cases
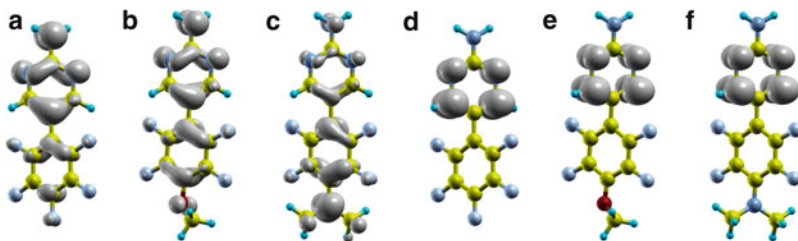
Fig. 5 Orbital character of the states HOMO (**a**)–(**c**) and LUMO (**d**)–(**f**) for FAP, OFAP and NFAP
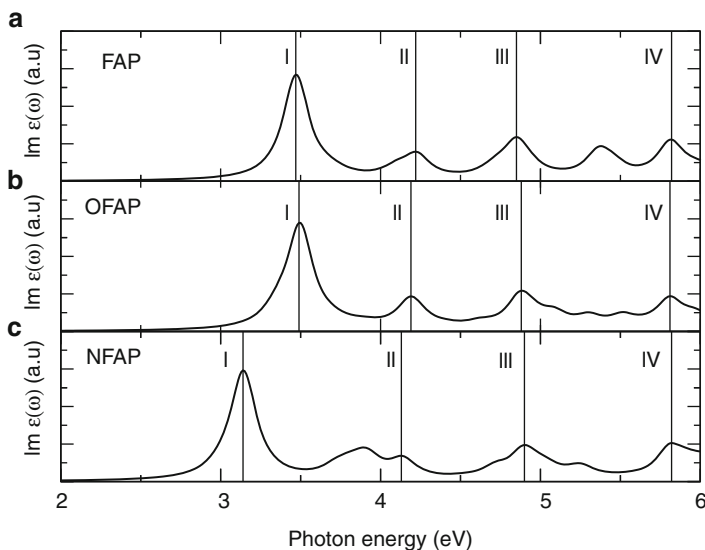

Fig. 6 Imaginary part of the dielectric function calculated in independent-particle approximation for FAP, OFAP and NFAP. A broadening of $\eta = 0.10\,\text{eV}$ has been used

the onset of the optical absorption is larger than $E_g^{DFT} = \varepsilon_L - \varepsilon_H$ due to the small transition probability between HOMO and LUMO. There are more similarities in the spectra. In particular FAP and OFAP agree largely concerning the positions and line shapes of the main peaks I-IV (see Fig. 6).

Since the dielectric function in independent-particle approximation is composed of independent transitions between occupied and empty electronic states, it is straightforward to interpret. In particular we find that transitions between HOMO and LUMO+1 are essentially causing the first absorption peak for all three molecules. The data show furthermore that the optical absorption occurs largely due to states localized at the aminopyrimidine and pentafluorophenyl rings. This explains why the optical response of the three molecules shown in Fig. 6 is rather similar. A notable exception is the first absorption peak of NFAP. In this case the HOMO is strongly influenced by amino-group localized states (cf. Fig. 5).
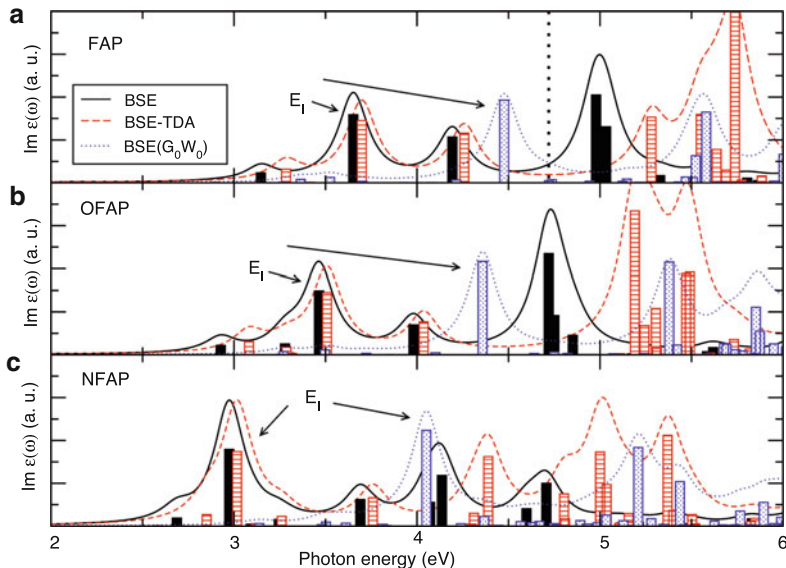
Fig. 7 Imaginary part of the dielectric function calculated by solving the BSE based on G_0W_0 calculations or by applying a respective scissors-shift to reproduce the ΔSCF-gaps or for FAP (**a**), OFAP (**b**) and NFAP (**c**). A broadening of $\eta = 0.10\,\text{eV}$ has been used. The *solid (dashed)/dotted curve* and *bars* gives the spectra and oszillator strengths versus the eigenvalues calculated within BSE (BSE-TDA) on the basis of the scissors shifted PW91/G_0W_0 electronic structure. The eigenvalues contributing to the first peak are labeled. See Ref. [23] for details. The strongest absorption maximum of FAP dissolved in ethanol[8] is shown by a *dotted line*

Contributions of the attached fluorine atom or the methoxy group are – to a much smaller extent – also present in the first absorption peak of FAP or OFAP (cf. Fig. 5).

In Fig. 7 the molecular dielectric functions calculated by taking many body effects into account are shown. The calculations have been performed using the full excitonic Hamiltonian as well as applying the TDA. The empty electronic levels were either shifted such that the respective molecular ΔSCF gaps are reproduced or the G_0W_0 electronic structure was used as input. The red-shift of the first peak in the NFAP spectra compared to FAP and OFAP as observed in IPA occurs also on the BSE level of theory. It is even enhanced by the smaller respective value of the ΔSCF gap. In general the positions of the first optical absorption maxima calculated within the BSE agree within 1 eV with the IPA calculation, which is indicative for some cancelation of quasi-particle and excitonic shifts as already concluded from the values in Table 1.

Similar to the IPA spectra discussed above we perform a systematic analysis of the states contributing to the respective absorption peaks (for details see Ref. [29]). It turns out that – as already found on the IPA level of theory – HOMO and LUMO+1 are the states that mostly contribute to the first adsorption peak.

Comparing the spectra obtained from the full Hamiltonian and in TDA one finds distinct differences: (i) a redshift of the eigenvalues going from TDA to the full

Hamiltonian and (ii) strong modifications of the line shape for energies above 4.5 eV (FAP, OFAP) or 4.0 eV (NFAP). While the Tamm-Dancoff-Approximation clearly affects the calculated optical absorption, in particular for excitations beyond the lowest absorption peak, we find the influence of the electronic structure that is used as input for the BSE calculations to be even more important. The optical spectrum based on the G_0W_0 electronic structure differs appreciable from the one based on scissors-shifted PW91 eigenvalues. This is due to the state-dependent self-energy corrections leading to an energetic reordering of the eigenvalue spectrum that results in a significant blue-shift of the optical absorption data.

The measured position of the optical absorption peak of FAP dissolved in ethanol[8] in the energy window 2.3–5.7 eV is at 4.72 eV (vertical line in Fig. 7). Clearly, the BSE spectrum based on the G_0W_0 electronic structure agrees best with this value. It yields an optical absorption peak at 4.48 eV. From Table 1 it is clear that the error bar of the calculated excitation energies is of the order of several tenths of an eV. Moreover, our choice for the static dielectric constant used in the molecule calculations is bound to result in excitation energies that approach the real values from below. An additional uncertainty in the experiment-theory comparison is related to the fact that the solvent molecules are not included in the present gas-phase calculations. Therefore the deviation between measured and calculated data of less than 0.3 eV is not surprising.

Comparing the computational results for the electronic states of FAP, OFAP, and NFAP summarized in Fig. 4 and the optical response from Figs. 6 and 7 one finds that the former are far more sensitive to the attachment of functional groups than the latter. Since the optical absorption essentially takes place at the aminopyrimidine and pentafluorophenyl rings, modifications in the molecular wave functions due to methoxy or amino group are only partially reflected in the optical data.

4   Summary

In the present work the electronic structure and optical response of 2-aminopyrimidines is analyzed on the basis of DFT as well as many-body perturbation theory calculations. The calculations predict quasiparticle gaps, i.e., differences between the ionization energies and electron affinities, of about 7 eV for the molecules. The energies of the lowest optical excitations of the respective molecules are considerably lower. In fact, our result indicates a near cancellation of the electronic self-energy and exciton binding energies for the lowest excitations of 2-aminopyrimidines. In addition to electron-hole attraction effects, we observe a very strong influence of local fields, i.e., the unscreened electron-hole exchange on the optical absorption spectra. Moreover, the resonant-nonresonant coupling terms in the excitonic Hamiltonian usually neglected in calculations for inorganic semiconductors are found to noticeably modify peak positions and oscillators strengths in case of the systems studied here.

References

1. M. Rohlfing, S.G. Louie, Phys. Rev. Lett. **81**, 2312 (1998)
2. S. Albrecht, L. Reining, R. DelSole, G. Onida, Phys. Rev. Lett. **80**, 4510 (1998)
3. M. Rohlfing, Int. J. Quant. Chem. **80**, 807 (2000)
4. G. Onida, L. Reining, A. Rubio, Rev. Mod. Phys. **74**, 601 (2002)
5. P.H. Hahn, W.G. Schmidt, F. Bechstedt, Phys. Rev. B **72**, 245425 (2005)
6. W.G. Schmidt, phys. stat. sol. (b) **242**, 2751 (2005)
7. I. Stoll, R. Brodbeck, B. Neumann, H.G. Stammler, J. Mattay, Crys. Eng. Comm. **11**(2), 306 (2009)
8. I. Stoll, R. Brockhinke, A. Brockhinke, M. Boettcher, T. Koop, H.G. Stammler, B. Neumann, A. Niemeyer, A. Huetten, J. Mattay, Chem. Materials **22**(16), 4749 (2010)
9. G. Kresse, J. Furthmüller, Comp. Mat. Sci. **6**, 15 (1996)
10. J.P. Perdew, J.A. Chevary, S.H. Vosko, K.A. Jackson, M.R. Pederson, D.J. Singh, C. Fiolhais, Phys. Rev. B **46**, 6671 (1992)
11. J. Heyd, G.E. Scuseria, M. Ernzerhof, J. Chem. Phys. **118**(18), 8207 (2003)
12. P.E. Blöchl, Phys. Rev. B **50**, 17953 (1994)
13. G. Kresse, D. Joubert, Phys. Rev. B **59**, 1758 (1999)
14. R.M. Dreizler, E.K.U. Gross, *Density Functional Theory* (Springer-Verlag, Berlin, 1990)
15. M. Preuss, W.G. Schmidt, K. Seino, J. Furthmüller, F. Bechstedt, J. Comp. Chem. **25**, 112 (2004)
16. A. Hermann, W.G. Schmidt, P. Schwerdtfeger, Phys. Rev. Lett. **100**, 207403 (2008)
17. M. Shishkin, G. Kresse, Phys. Rev. B **74**, 035101 (2006)
18. H. Ehrenreich, M.H. Cohen, Phys. Rev. **115**, 786 (1959)
19. S.L. Adler, Phys. Rev. **126**, 413 (1962)
20. N. Wiser, Phys. Rev. **129**, 62 (1963)
21. V. Olevano, L. Reining, Phys. Rev. Lett. **86**, 5962 (2001)
22. F. Bechstedt, R. Del Sole, G. Cappellini, L. Reining, Solid State Commun. **84**, 765 (1992)
23. A. Riefer, F. Fuchs, C. Rödl, A. Schleife, F. Bechstedt, R. Goldhahn, Phys Rev B **84**(7), 075218 (2011)
24. W.G. Schmidt, M. Albrecht, S. Wippermann, S. Blankenburg, E. Rauls, F. Fuchs, C. Rödl, J. Furthmüller, A. Hermann, Phys. Rev. B **77**, 035106 (2008)
25. P.H. Hahn, W.G. Schmidt, K. Seino, M. Preuss, F. Bechstedt, J. Bernholc, Phys. Rev. Lett. **94**, 037404 (2005)
26. W.G. Schmidt, S. Glutsch, P.H. Hahn, F. Bechstedt, Phys. Rev. B **67**, 085307 (2003)
27. A. Ruini, M. Caldas, G. Bussi, E. Molinari, Phys. Rev. Lett **88**(20) (2002)
28. A.Y. Golovacheva, A.N. Romanov, V.B. Sulimov, J. Phys. Chem. A **109**, 3244 (2005)
29. A. Riefer, E. Rauls, W.G. Schmidt, J. Eberhard, I. Stoll, J. Mattay, Phys Rev B **85**, 165202 (2012)